

Letter

Enhanced Photocatalytic Efficiency of TiO₂ Membrane Decorated with Ag and Au Nanoparticles

Yining Gao ¹, Wenqin Zhang ^{1,*} and Peng Liu ²

¹ State Key Laboratory of Silicate Materials for Architectures, Wuhan University of Technology, Wuhan 430070, China; gyn@whut.edu.cn

² School of Chemistry, Chemical Engineering and Life Science, Wuhan University of Technology, Wuhan 430070, China; chemliup@whut.edu.cn

* Correspondence: wqzhang@whut.edu.cn

Received: 9 May 2018; Accepted: 25 May 2018; Published: 7 June 2018



Featured Application: The photocatalysis could be used for water treatment and other environmental engineering.

Abstract: Ag and Au nanoparticles (NPs) were decorated on the surface of TiO₂ membranes by two methods, i.e., hydrothermal synthesis and photoreduction. The size of Ag and Au NPs on the surface of TiO₂ membranes was dependent on the method of preparation and varied from 2 nm–10 nm. The photocatalytic performance of the TiO₂ particle, TiO₂ membrane and the Ag/Au-decorated TiO₂ membrane was tested for the catalytic degradation of Rhodamine B (RhB) and *Escherichia coli* (*E. coli*) under irradiation of visible light. The experiment results showed that both Ag- and Au-decorated TiO₂ membranes exhibited excellent photocatalytic activity in the visible light region. Among the prepared materials, Ag-decorated TiO₂ membranes prepared by photoreduction showed the highest activity, which could be attributed to the local surface plasmon resonance (LSPR) effect of the noble metal.

Keywords: TiO₂ membrane; Ag decoration; photocatalyst; visible light irradiation; *Escherichia coli*

In recent years, many thin film materials, including carbon film, graphene and thin SnO₂ membranes, have been studied and have shown excellent physical and chemical properties [1–3]. Various TiO₂ nanomaterials have also been reported, such as TiO₂ nanopowders, nanowires, nanotubes, nanoflowers, etc. [4–6]. Among them, TiO₂ membrane have gained considerable attention due to their outstanding catalytic performance, which could be attributed to the large surface area and low thickness of the material [7,8]. TiO₂ nanoparticles (NPs) with a large specific area have higher photocatalytic efficiency because the photocatalytic process occurs on the surface.

High photocatalytic efficiency is the main evaluation method for photocatalysts, which is important to degrade organics in short time periods [9,10]. According to the research, photocatalysts with low photocatalytic efficiency degraded organics within a couple of hours, such as nitrogen-doped TiO₂ thin film [11], TiO₂ nanotubes [12] and BiOCl nanowire arrays [13]; high photocatalytic efficiency like that of BiOCl membranes could completely degrade RhB within 2 min under UV light [14].

Further modification of TiO₂ can improve its response to visible light, inhibit the recombination of photogenerated carriers and, consequently, enhance the photocatalytic performance. Various materials, including metals (Au, Ag, Pt, Cu), non-metals (C, N, S), metal oxides (WO₃, Fe₂O₃, SiO₂), etc., have been used to dope TiO₂ [8,15–17]. These doping materials can produce vacancies and interstitial or substitutional defects that change the photocatalytic properties of TiO₂. The band gap of TiO₂ is narrowed notably after doping with noble metals (Au, Ag, Pt) [18]. Because the noble metals have lower Fermi levels than TiO₂, the photogenerated electrons of the conduction band will not

recombine with the holes, but instead transfer to the noble metal particles on the surface of TiO₂ [19–22]. Hence, the photogenerated electrons and holes are effectively separated, and the photocatalytic activity is improved [23–25]. Moreover, the noble metal NPs can more easily attract organic molecules than semiconductors. Therefore, the noble metal NPs play the role of the electron carrier in the system of TiO₂ doped with noble metals, which is an effective method to improve the photocatalytic properties of TiO₂.

Herein, we report a TiO₂ membrane decorated with Ag and Au NPs, which exhibited extremely high catalytic efficiency. The TiO₂ membrane was prepared by a hydrothermal method [26]. A certain amount (8 mL) of TiCl₃ was mixed with ethylene glycol (30 mL), and the mixture was stirred for 7 h at room temperature until the reaction completed. Then, doubly-distilled water (1 mL) was added, and the mixture was transferred into a stainless steel reactor and kept at 150 °C for 4 h. The products were separated by centrifugation at 16,000 rpm, washed with ethanol three times and dried in a vacuum at 50 °C for 48 h. TiO₂ membrane was decorated with Ag and Au NPs by the hydrothermal and photoreduction methods, respectively. The mixture of the TiO₂ membrane (0.4 mg) and AgNO₃ or HAuCl₄ (0.015 mol/L, 0.4 mL) was processed by 365-nm UV light or hydrothermal reaction (180 °C, 6 h). The final products were centrifuged at 10,000 rpm, washed with doubly-distilled water three times and dried in a vacuum at 50 °C for 24 h. The sample descriptions are given in Table 1.

Table 1. Processes for TiO₂ membranes.

Name	Sample Description	Process Method	Ti (At%)	Ag (At%)	Au (At%)
S ₀	TiO ₂ membrane		–	–	–
S _{Ag-UV}	TiO ₂ membrane with Ag	UV	48.2	1.1	–
S _{Ag-HY}	TiO ₂ membrane with Ag	hydrothermal reaction	47.7	2.0	–
S _{Au-UV}	TiO ₂ membrane with Au	UV	48.1	–	1.2
S _{Au-HY}	TiO ₂ membrane with Au	hydrothermal reaction	47.6	–	2.3

TiO₂ membranes decorated with Ag and Au NPs were observed and characterized by transmission electron microscope (TEM, Talos F200S, Thermo fisher, Waltham, MA, USA) and X-ray diffraction (XRD, PHILIPS P W 3040/60X'PertPRO, Amsterdam, The Netherlands). Scanning electron microscope energy dispersive spectromete (SEM EDS, JSM-7500F, JEOL Ltd., Tokyo, Japan) analysis showed the real composition of the prepared samples, as given in Table 1. Ultraviolet-visible light (UV-Vis) diffuse reflectance spectroscopy was measured on a Perkin Elmer UV-Vis spectrometer (Lambda 750 S, Perkin Elmer, Waltham, MA, USA) equipped with a Labsphere RSA-PE-20 integration sphere. The electrochemical behaviors of the TiO₂ membranes, S_{Ag} and S_{Au}, were examined by electrochemical impedance spectroscopy (EIS, RST5200F, shiruisi Instrument, Zhengzhou, China). The photocatalytic performance of the TiO₂ membranes, S_{Ag} and S_{Au}, was evaluated by the degradation reaction of Rhodamine B (RhB). A Xe lamp with optical filters (14 V, 14–21 A, visible light) was used as the light source, and the distance between the lamp and the interface of the solution was 12 cm (0.1 W/m²). The test was carried out by adding the prepared photocatalyst (0.4 mg) to the solution of RhB (5 mg/L, 250 mL) and measuring the absorbance at 552 nm (i.e., the maximum absorption wavelength of RhB) by UV-visible spectrophotometry every 5 min. The concentration of RhB in the solution was calculated from the absorbance, and the photocatalytic degradation efficiency was calculated as follows:

$$\eta = \frac{C_0 - C_t}{C_0} \quad (1)$$

where C₀ is the initial concentration of RhB and C_t is the concentration of RhB after an irradiation time of t. *Escherichia coli* (*E. coli*) cells were treated by S_{Ag} under visible light irradiation (0.1 W/m²) for 10 min. Then, the morphology of the native and treated *E. coli* cells was examined by SEM. The cells were fixed according to the standard protocol by reduction with glutaraldehyde and oxidation with OsO₄, then dehydrated stepwise with ethanol of increasing concentration (50–100%).

The prepared TiO₂ membrane was decorated with Ag/Au NPs by either hydrothermal synthesis or photoreduction. The morphology and structure of the resulting material were observed and characterized by TEM. Figure 1 shows the diameter histogram and the TEM images of the S_{Ag} and S_{Au} samples prepared under different conditions.

The ultrathin TiO₂ membrane was two atoms thick and Ag or Au NPs were dispersed on the membrane surface, as shown in Figure 1. The particle size ranged from 2 nm–10 nm. The particle size of the decorated Ag was the smallest (ca. 2 nm) when S_{Ag} was prepared by photoreduction with ultraviolet light (Figure 1). Similarly, the particle size of the decorated Au was also the smallest (ca. 2 nm) in S_{Au} prepared by photoreduction with ultraviolet light (Figure 2D). Hydrothermal synthesis at 180 °C furnished Au particles of ca. 10 nm in size on the TiO₂ membrane. Ag or Au NPs prepared by the photoreduction method were dispersed evenly within the TiO₂ network. However, the NPs aggregated together with hydrothermal synthesis. Generally, Ag and Au NPs were successfully decorated on the TiO₂ membrane.

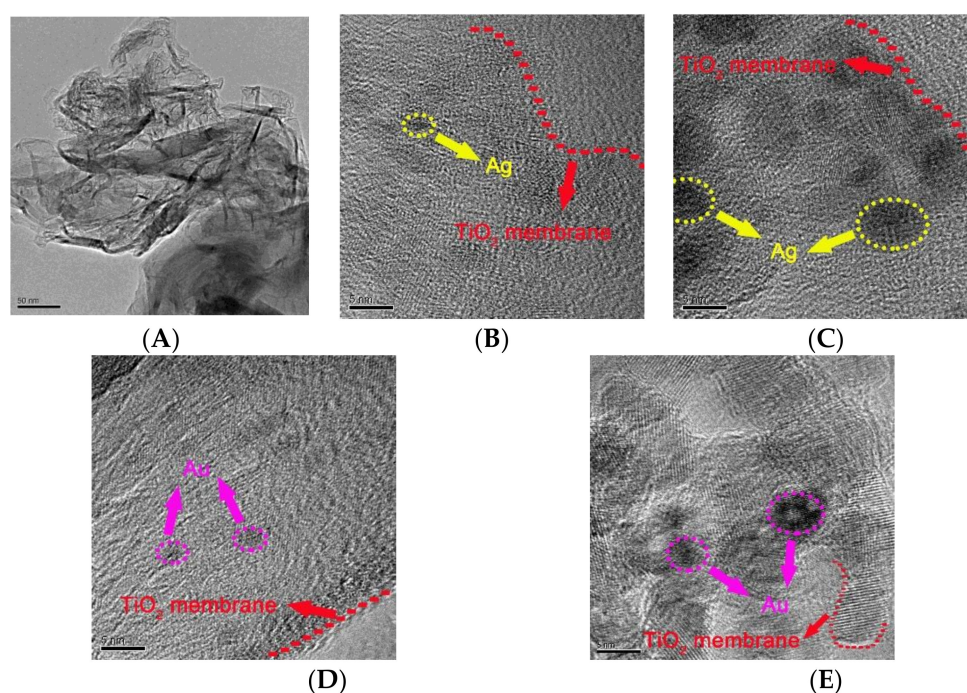


Figure 1. TEM images of the TiO₂ membrane and those decorated with Ag or Au NPs. (A) TiO₂ membrane; (B) TiO₂ membrane decorated with Ag NPs by UV irradiation; (C) TiO₂ membrane decorated with Ag NPs by hydrothermal synthesis; (D) TiO₂ membrane decorated with Au NPs by UV irradiation; (E) TiO₂ membrane decorated with Au NPs by hydrothermal synthesis.

The S_{Ag} and S_{Au} samples exhibited some adsorption in the visible light region as shown in Supplementary Material S1, which could be attributed to the local surface plasmon resonance (LSPR) of the Ag and Au NPs. The LSPR effect on the surface of noble metal NPs is caused by the collective shock of conductive electrons generated by electromagnetic radiation. The size and shape of the noble metal NPs can change the surface density of the electromagnetic field and are thus important factors for the LSPR effect [27]. Obviously, the S_{Ag} sample prepared by photoreduction had a strong absorption in the visible light region. For TiO₂, the absorption in the UV region resulted only from its wide band gap (3.2 eV). After the Ag and Au NPs were introduced, the light response range of TiO₂ clearly extended to the visible region. The Ag and Au NPs on the TiO₂ membrane could transfer free electrons generated by the LSPR effect to the valence band of TiO₂ and consequently enhance the photocatalytic activity of TiO₂ under visible light [28–30].

Figure 2 shows the photocatalytic degradation of RhB with P25 (TiO_2 particle with size 25 nm) and the decorated TiO_2 membrane. The degradation efficiency of RhB was evaluated by the first order reaction, which is presented in Supplementary Material S2. The catalytic efficiency of photocatalysts was ranked as $S_{\text{Ag-UV}} > S_{\text{Ag-HY}} > S_{\text{Au-UV}} > S_{\text{Au-HY}} > S_0 > S_{\text{P25}}$. When P25 was used as the catalyst, the degradation of RhB under irradiation of visible light was very limited. Nevertheless, the degradation efficiency was improved notably when the TiO_2 membrane was used in the photodegradation reaction. The decorated TiO_2 membrane enhanced the degradation efficiency further. S_{Ag} exhibited higher catalytic efficiency than S_{Au} . Besides, $S_{\text{Ag}}/S_{\text{Au}}$ prepared by UV irradiation exhibited higher degradation efficiency than hydrothermal synthesis. In addition, the recycling experiment of $S_{\text{Ag-UV}}$ showed that it could be used over 50 times and that the photocatalytic efficiency of $S_{\text{Ag-UV}}$ had not reduced significantly, which is presented in Supplementary Material S3.

Mechanistically, in the photocatalytic reaction, photogenerated electrons and holes on the TiO_2 membrane work as the active species to decomposing organic compounds. The existence of Ag and Au NPs on the TiO_2 membrane forms a Schottky junction on the surface of TiO_2 , which promotes charge separation and improves the quantum efficiency. Generally, Ag shows a stronger LSPR effect than Au. In addition, the absorption range of TiO_2 extended to the visible light region due to the LSPR effect of the Ag and Au NPs. Since the LSPR sensitization effect of plasmonic NPs depends mainly on their size and shape, the LSPR effect is strengthened when the size of the Ag and Au NPs increases [31,32]. Hence, the S_{Au} and S_{Ag} samples prepared by photoreduction showed higher efficiency in the photodegradation of RhB. During this process, RhB was first broken down into benzoic acid and phthalic acid and then into ethanedioic acid, while the organic carbon content remain unchanged [33]. Finally, the RhB was degraded into small molecules, such as CO_2 , NO_x and H_2O , and finally, oxidized completely, with the organic carbon content decreased significantly [34–36].

The degradation of RhB by photocatalysts has been reported by many groups. TiO_2 and Fe_2O_3 co-doped graphene aerogel can remove 97.7% RhB within 60 min under visible light irradiation [37]. SiO_2/C -doped TiO_2 hollow spheres can degrade 61.7% RhB after 100 min under UV irradiation [38]. Ag/ TiO_2 composites can degrade 80% RhB after 120 min under UV irradiation [39]. Compared with the above photocatalysts, the Ag decorated TiO_2 membrane can almost degrade 90% RhB within 30 min under visible light irradiation. Therefore, Ag/Au-decorated TiO_2 membranes showed excellent photodegradation efficiency.

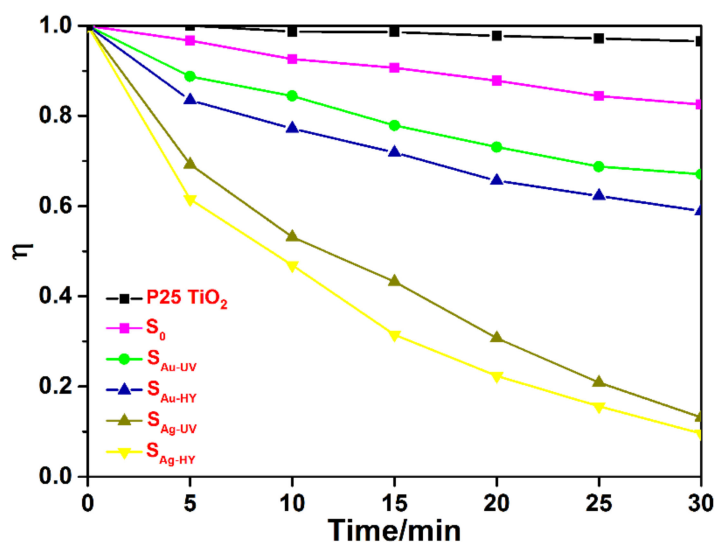


Figure 2. Photocatalytic degradation of RhB by TiO_2 membrane decorated with Ag and Au NPs.

The prepared TiO_2 membrane was characterized as being two atoms thick [26]. The specific surface area was greatly increased compared with P25 TiO_2 . The target molecules were more easily

absorbed on TiO₂ membrane. The degradation of the target molecules experienced a dynamic adsorption-photocatalysis-desorption process. The electron and hole produced under irradiation reacted with the target molecules on the enlarged surface; thus, the recombination of the electron and hole was also inhibited. The process is presented in Figure 3. As a result, the photocatalytic efficiency of the TiO₂ membrane was enhanced significantly compared to P25 TiO₂.

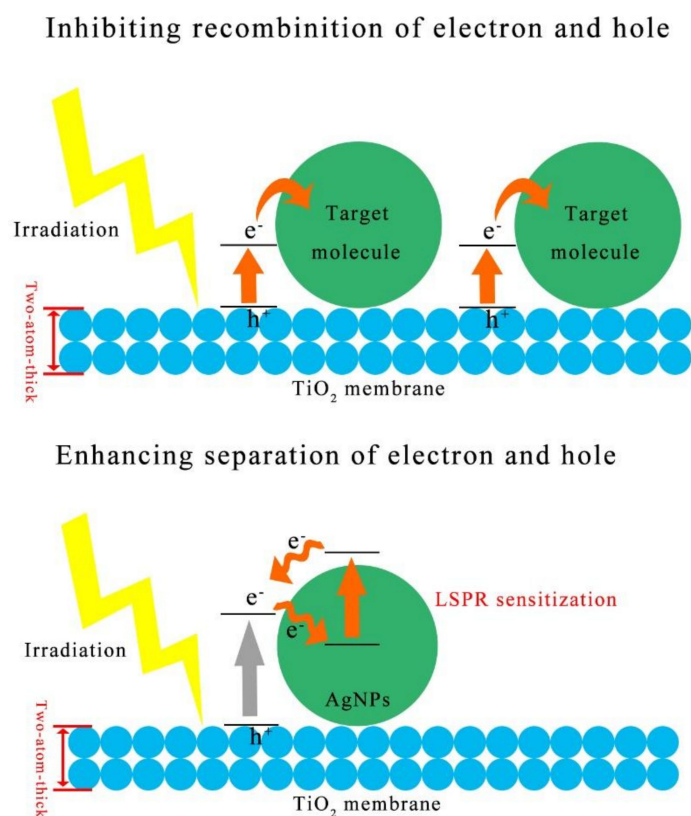


Figure 3. Scheme of the mechanism of inhibiting the recombination of electrons and holes by TiO₂ membranes and enhancing the separation of electrons and holes.

The photocatalytic mechanism is demonstrated below with S_{Ag} as an example. The S_{Au} has photoresponse in the visible light region due to the LSPR effect of Au NPs. Analyzing by EIS, the Au NP-doped TiO₂ membrane represented lower resistances than the pure TiO₂ membrane, which could make the charge transfer at the interface more rapid and effective. The charges on the surface of Au NPs are subjected to collective shock under irradiation of visible light and become free electrons, which results in a strengthened local electric field. Under the local electric field, free electrons then rapidly jump to the conduction band (CB) of TiO₂ and overcome the Schottky junction, which results in the separation of photogenerated electrons and holes and thus improves quantum efficiency. Generally, pure TiO₂ has a wide band gap. Under light irradiation, the excitation of an electron would take place if the light energy is greater than the band gap of the catalysts. The wide band gap of pure TiO₂ is known to be 3.2 eV. By using Mott–Schottky plots and XPS spectra, the band gap from the valence band to the conduction band for Ag-decorated TiO₂ decreased to 2.6 eV. Therefore, the material showed photocatalytic activity under visible light irradiation. The photogenerated electrons can react with the O₂ on the surface of catalyst to form ·O₂[−], and the holes of Au can combine with H₂O on the catalyst surface to form ·OH, both of which are strongly oxidative. These oxidative species can then oxidize the RhB molecule on the surface of Au NPs.

The photocatalysis degradation is divided into three stages. They are the formation of both the hole and electron under light excitation, the production of radical species and the reaction of the

radical species with the targets (pollutants, bacteria, etc.). Electron paramagnetic resonance (EPR) has confirmed the separation of the hole and electron [40]. The production of radical species along time was also proven by the different adduct species detected with EPR [41]. The degradation product of the targets was detected by some groups [42]. The silver content is closely related to the separation of the hole and electron and the production of radical species, as described above. As a result, silver will affect photocatalysis and degradation efficiency significantly.

Au or Ag NPs experience an evolution during the photocatalytic process. A moderate growth of particle size was observed. From the statistics of the TEM images, the particle size of Ag and Au NPs increased from 2.3 ± 0.1 nm– 13 ± 0.3 nm and from 2.4 ± 0.1 nm– 17 ± 0.4 nm after photocatalysis, respectively. On the other hand, the photocatalytic activity did not change in the catalyst recyclability test (Supplementary Material S3), showing that Au or Ag NPs maintain a dominant metallic state.

The surface morphology of the *E. coli* cells was examined by SEM. Figure 4A shows that the native *E. coli* cells had a rod-like structure with regular wrinkles, which was changed after the photocatalytic degradation. Figure 4B shows that some depressions appeared on the surface of cells treated with P25 TiO₂, and irregular wrinkles appeared on the cells treated with S_{Au}.

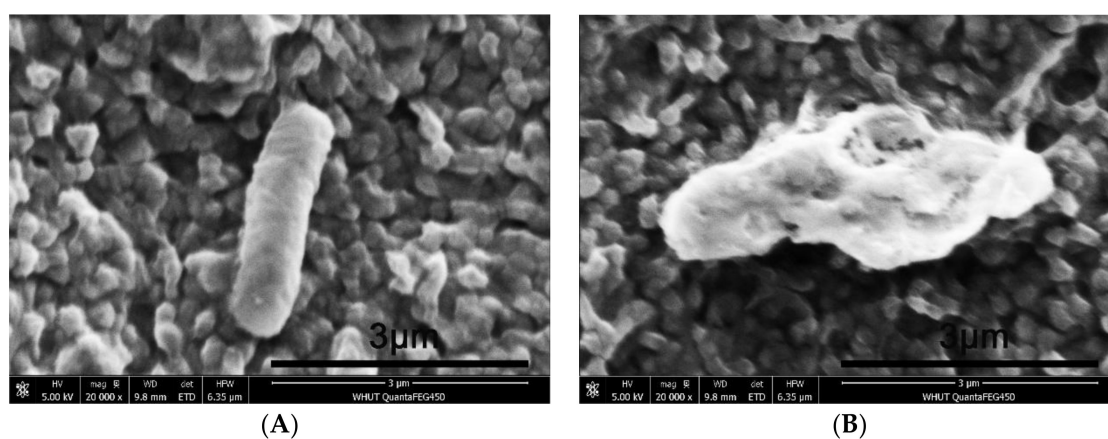


Figure 4. SEM images of the native (A) and treated *E. coli* cells (B) with a scale bar (3 μ m).

The results suggested that the cell surface was damaged and the cell membrane structure was altered. The outer membrane of Gram-negative bacteria is composed of lipopolysaccharide (LPS), peptidoglycan and phospholipid layers. The mechanical strength of the cell membrane depends on peptidoglycan, and LPS is responsible for the surface structure and morphology [43–45]. The beta 1,4-link between the two amino sugars of *N*-acetyl glucose amine and *N*-acetyl acid forms the LPS. By connecting four peptide side chains on the *N*-acetyl cell wall acid molecules, the peptides in between are again joined by bridges to form a reticulate structure that is very strong. Therefore, the cell membrane plays a vital role in maintaining cell morphology. The outermost layer of the cell membrane is LPS, which is exposed to the environment and subjected to the attack of free radicals during photocatalytic degradation. The cells still maintained the original rod shape after treatment with P25 TiO₂ and S_{Au}, which indicated that LPS was damaged, but peptidoglycan remained intact. The peptidoglycan layer and the outer membrane form a strong network to maintain the morphology of the cell [46,47]. In contrast, after treatment with S_{Ag}, the *E. coli* cells exhibited a fusiform structure, and the structure of the native cells was destroyed, which indicated that the outer membrane and the peptidoglycan layer were fully damaged, but the inner membrane remained intact. In addition, *E. coli* photo-killing analysis was done by *E. coli* inactivation, suggesting that the *E. coli* treated with S_{Ag} inactivation was decreased within 3.5 h under visible light, which is presented in Supplementary Material S4.

The outstanding performance of the TiO₂ membrane as a photocatalyst stems from the material's large surface area and small thickness. However, the quantum efficiency of the TiO₂ membrane

is not high. Decorating the TiO₂ membrane with Ag and Au NPs can extend the photo response to a broader range and improve the photocatalytic properties. In this work, the TiO₂ membrane was prepared by hydrothermal synthesis, and then, Ag and Au NPs were decorated on the surface of the TiO₂ membrane by hydrothermal synthesis or photoreduction. The size of the Ag and Au NPs prepared by photoreduction was ca. 2 nm and the smallest among all material samples (Supplementary Material S5). The size of the noble metal NPs is important for the local surface plasmon resonance (LSPR) sensitization and affects the quantum efficiency. Under visible light, S_{Ag} and S_{Au} showed excellent photocatalytic performance. Silver NPs can produce a stronger LSPR effect than Au NPs [31,32]. The TiO₂ membranes decorated with Ag NPs were found to have good photocatalytic properties in the degradation of RhB and *E. coli* under irradiation of visible light and presumably may find use in the photocatalytic degradation of more organic compounds and microorganisms.

Supplementary Materials: The following are available online at <http://www.mdpi.com/2076-3417/8/6/945/s1>. Figure S1. UV-Vis diffuse reflectance spectroscopy of S0, SAg-UV, SAg-HY, SAu-UV, SAu-HY and P25 TiO₂. Table S2. Degradation rate constant of Rhodamine B. Figure S3. Recycling test of the SAg-UV during the degradation of RhB under visible light irradiation. Figure S4. *E. coli* inactivation with SAg treatment. Figure S5. The evolution of Au or Ag NPs' particle size after the photocatalytic process. The particle size of Ag and Au NPs increased from 2.3 ± 0.1 nm–13 ± 0.3 nm and from 2.4 ± 0.1 nm–17 ± 0.4 nm, respectively.

Author Contributions: W.Z. and F.W. conceived and designed the experiments; Y.G. performed the experiments; P.L. and Y.G. analyzed the data; F.W. contributed reagents/materials/analysis tools; W.Z. and Y.G. wrote the paper.

Acknowledgments: This work was financially supported by the National Natural Science Foundation of China (Grant No. 51502222).

Conflicts of Interest: The authors declare no conflict of interest.

References

1. Brilot, A.F.; Chen, J.Z.; Cheng, A.; Pan, J.; Harrison, S.C.; Potter, C.S.; Carragher, B.; Henderson, R.; Grigorieff, N. Beam-induced motion of vitrified specimen on holey carbon film. *J. Struct. Biol.* **2012**, *177*, 630–637. [[CrossRef](#)] [[PubMed](#)]
2. Di Valentin, C.; Pacchioni, G.; Selloni, A.; Livraghi, S.; Giamello, E. Characterization of Paramagnetic Species in N-Doped TiO₂ Powders by EPR Spectroscopy and DFT Calculations. *J. Phys. Chem. B* **2005**, *109*, 11414–11419. [[CrossRef](#)] [[PubMed](#)]
3. Brennan, B.; Spencer, S.J.; Belsey, N.A.; Faris, T.; Cronin, H.; Silva, S.R.P.; Sainsbury, T.; Gilmore, I.S.; Stoeva, Z.; Pollard, A.J. Structural, chemical and electrical characterisation of conductive graphene-polymer composite films. *Appl. Surf. Sci.* **2017**, *403*, 403–412. [[CrossRef](#)]
4. Mor, G.K.; Carvalho, M.A.; Varghese, O.K.; Pishko, M.V.; Grimes, C.A. A room-temperature TiO₂-nanotube hydrogen sensor able to self-clean photoactively from environmental contamination. *J. Mater. Res.* **2004**, *19*, 628–634. [[CrossRef](#)]
5. Lei, Y.; Zhang, L.D.; Meng, G.W.; Li, G.H. Preparation and photoluminescence of highly ordered TiO₂ nanowire arrays. *Appl. Phys. Lett.* **2001**, *78*, 1125–1127. [[CrossRef](#)]
6. Xia, H.R.; Peng, C.; Li, J.; Sun, W.T.; Ai, G.; Peng, L.M. Large-scale floated single-crystalline TiO₂ flower-like films: synthesis details and applications. *RSC Adv.* **2013**, *3*, 17668–17671. [[CrossRef](#)]
7. Xiang, G.; Li, T.; Zhuang, J.; Wang, X. Large-scale synthesis of metastable TiO₂(B) membrane with atomic thickness and their photocatalytic properties. *Chem. Commun.* **2010**, *46*, 6801–6803. [[CrossRef](#)] [[PubMed](#)]
8. Choi, H.; Stathatos, E.; Dionysiou, D.D. Photocatalytic TiO₂ films and membranes for the development of efficient wastewater treatment and reuse systems. *Desalination* **2015**, *202*, 199–206. [[CrossRef](#)]
9. Ma, R.; Islam, M.J.; Reddy, D.A.; Kim, T.K. Transformation of CeO₂ into a mixed phase CeO₂/Ce₂O₃ nanohybrid by liquid phase pulsed laser ablation for enhanced photocatalytic activity through Z-scheme pattern. *Ceram. Int.* **2016**, *42*, 18495–18502. [[CrossRef](#)]
10. Islam, M.J.; Kim, H.K.; Reddy, D.A.; Kim, Y.; Ma, R.; Baek, H.; Kim, J.; Kim, T.K. Hierarchical BiOI nanostructures supported on a metal organic framework as efficient photocatalysts for degradation of organic pollutants in water. *Dalton Trans.* **2017**, *46*, 6013–6023. [[CrossRef](#)] [[PubMed](#)]
11. Irie, H.; Washizuka, S.; Watanabe, Y.; Kako, T.; Hashimoto, K. Photoinduced Hydrophilic and Electrochemical Properties of Nitrogen-Doped TiO₂ Films. *J. Electrochem. Soc.* **2005**, *152*, E351–E356. [[CrossRef](#)]

12. Chen, Y.; Shi, L.Y.; Yuan, S. Photoelectrocatalytic Degradation of Methylene Blue by TiO₂ Nanotube. *J. Inorg. Mater.* **2009**, *24*, 680–684. [[CrossRef](#)]
13. Wu, S.; Wang, C.; Cui, Y.; Wang, T.; Huang, B.; Zhang, X.; Qin, X.; Brault, P. Synthesis and photocatalytic properties of BiOCl nanowire arrays. *Mater. Lett.* **2010**, *64*, 115–118. [[CrossRef](#)]
14. Ye, L.; Zan, L.; Tian, L.; Peng, T.; Zhang, J. The {001} Facets-Dependent High Photoactivity of BiOCl Membrane. *Chem. Commun.* **2011**, *47*, 6951–6953. [[CrossRef](#)] [[PubMed](#)]
15. Wang, C.; Zhou, Y.; Ge, M.; Xu, X.; Zhang, Z.; Jiang, J.Z. Large-scale synthesis of SnO₂ membrane with high lithium storage capacity. *J. Am. Chem. Soc.* **2010**, *132*, 46–47. [[CrossRef](#)] [[PubMed](#)]
16. Kumar, S.G.; Devi, L.G. Review on modified TiO₂ photocatalysis under UV/Visible light: selected results and related mechanisms on interfacial charge carrier transfer dynamics. *J. Phys. Chem. A* **2011**, *115*, 13211–13241. [[CrossRef](#)] [[PubMed](#)]
17. Daghrir, R.; Drogui, P.; Robert, D. Modified TiO₂ for Environmental Photocatalytic Applications: A Review. *Ind. Eng. Chem. Res.* **2013**, *52*, 3581–3599. [[CrossRef](#)]
18. Finazzi, E.; Valentin, C.D.; Pacchioni, G.; Selloni, A. Excess electron states in reduced bulk anatase TiO₂: Comparison of standard GGA, GGA+U, and hybrid DFT calculations. *J. Chem. Phys.* **2008**, *129*, 035108. [[CrossRef](#)] [[PubMed](#)]
19. Reddy, D.A.; Choi, J.; Lee, S.; Kim, T.K. Synthesis of heterostructured Ag@AgI/ZnS microspheres with enhanced photocatalytic activity and selective separation of methylene blue from mixture dyes. *J. Taiwan Inst. Chem. Eng.* **2016**, *66*, 200–209. [[CrossRef](#)]
20. Islam, M.J.; Reddy, D.A.; Han, N.S.; Choi, J.; Song, J.K.; Kim, T.K. An oxygen-vacancy rich 3D novel hierarchical MoS₂/BiOI/AgI ternary nanocomposite: Enhanced photocatalytic activity through photogenerated electron shuttling in a Z-scheme manner. *Phys. Chem. Chem. Phys.* **2016**, *18*, 24984–24993. [[CrossRef](#)] [[PubMed](#)]
21. Islam, M.J.; Reddy, D.A.; Choi, J.; Kim, T.K. Surface oxygen vacancy assisted electron transfer and shuttling for enhanced photocatalytic activity of a Z-scheme CeO₂-AgI nanocomposite. *RSC Adv.* **2016**, *6*, 19341–19350. [[CrossRef](#)]
22. Rahimi, N.; Pax, R.A.; Gray, E.M. Review of functional titanium oxides. I: TiO₂ and its modifications. *Prog. Solid State Chem.* **2016**, *44*, 86–105. [[CrossRef](#)]
23. Lee, S.; Reddy, D.A.; Kim, T.K. Well-wrapped reduced graphene oxide nanosheets on Nb₃O₇(OH) nanostructures as good electron collectors and transporters for efficient photocatalytic degradation of rhodamine B and phenol. *RSC Adv.* **2016**, *6*, 37180–37188. [[CrossRef](#)]
24. Reddy, D.A.; Choi, J.; Lee, S.; Ma, R.; Kim, T.K. Green Synthesis of AgI Nanoparticle-Functionalized Reduced Graphene Oxide Aerogels with Enhanced Catalytic Performance and Facile Recycling. *RSC Adv.* **2015**, *5*, 67394–67404. [[CrossRef](#)]
25. Islam, M.J.; Reddy, D.A.; Ma, R.; Kim, Y.; Kim, T.K. Reduced-graphene-oxide-wrapped BiOI-AgI heterostructured nanocomposite as a high-performance photocatalyst for dye degradation under solar light irradiation. *Solid State Sci.* **2016**, *61*, 32–39. [[CrossRef](#)]
26. Liu, P.; Zhao, Y.; Qin, R.; Mo, S.; Chen, G.; Gu, L.; Chevrier, D.M.; Zhang, P.; Guo, Q.; Zang, D. Photochemical route for synthesizing atomically dispersed palladium catalysts. *Science* **2016**, *352*, 797–800. [[CrossRef](#)] [[PubMed](#)]
27. Sarina, S.; Waclawik, E.R.; Zhu, H. ChemInform Abstract: Photocatalysis on Supported Gold and Silver Nanoparticles under Ultraviolet and Visible Light Irradiation. *Cheminform* **2013**, *44*, 1814–1833. [[CrossRef](#)]
28. Zhou, X.; Liu, G.; Yu, J.; Fan, W. Surface plasmon resonance-mediated photocatalysis by noble metal-based composites under visible light. *J. Mater. Chem.* **2012**, *22*, 21337–21354. [[CrossRef](#)]
29. Bera, S.; Ji, E.L.; Rawal, S.B.; Wan, I.L. Size-dependent plasmonic effects of Au and Au@SiO₂ nanoparticles in photocatalytic CO₂ conversion reaction of Pt/TiO₂. *Appl. Catal. B Environ.* **2016**, *199*, 55–63. [[CrossRef](#)]
30. Choi, J.; Reddy, D.A.; Islam, M.J.; Ma, R.; Kim, T.K. Self-assembly of CeO₂, nanostructures/reduced graphene oxide composite aerogels for efficient photocatalytic degradation of organic pollutants in water. *J. Alloys Compd.* **2016**, *688*, 527–536. [[CrossRef](#)]
31. Zhang, X.; Chen, Y.L.; Liu, R.S.; Tsai, D.P. Plasmonic photocatalysis. *Rep. Prog. Phys.* **2013**, *76*, 046401. [[CrossRef](#)] [[PubMed](#)]

32. Zheng, Z.; Huang, B.; Qin, X.; Zhang, X.; Dai, Y.; Whangbo, M.H. Facile in situ synthesis of visible-light plasmonic photocatalysts M@TiO₂ (M = Au, Pt, Ag) and evaluation of their photocatalytic oxidation of benzene to phenol. *J. Mater. Chem.* **2011**, *21*, 9079–9087. [[CrossRef](#)]
33. Li, J.Y.; Ma, W.H.; Lei, P.X.; Zhao, P.C. Detection of intermediates in the TiO₂-assisted photodegradation of Rhodamine B under visible light irradiation. *J. Environ. Sci.* **2007**, *19*, 892–896. [[CrossRef](#)]
34. Reddy, D.A.; Ma, R.; Choi, M.Y.; Kim, T.K. Reduced graphene oxide wrapped ZnS–Ag₂S ternary composites synthesized via hydrothermal method: Applications in photocatalyst degradation of organic pollutants. *Appl. Surf. Sci.* **2015**, *324*, 725–735. [[CrossRef](#)]
35. Reddy, D.A.; Lee, S.; Choi, J.; Park, S.; Ma, R.; Yang, H.; Kim, T.K. Green synthesis of AgI-reduced graphene oxide nanocomposites: Toward enhanced visible-light photocatalytic activity for organic dye removal. *Appl. Surf. Sci.* **2015**, *341*, 175–184. [[CrossRef](#)]
36. Choi, J.; Reddy, D.A.; Kim, T.K. Enhanced photocatalytic activity and anti-photocorrosion of AgI Nanostructures by coupling with graphene-analogue boron nitride nanosheets. *Ceram. Int.* **2015**, *41*, 13793–13803. [[CrossRef](#)]
37. Zhang, J.J.; Qi, P.; Zheng, X.C.; Liu, P.; Guan, X.X.; Zheng, G.P. Three-dimensional Fe₂O₃-TiO₂-graphene aerogel nanocomposites with enhanced adsorption and visible light-driven photocatalytic performance in the removal of RhB dyes. *J. Ind. Eng. Chem.* **2017**, *61*, 407–415. [[CrossRef](#)]
38. Zhang, Y.; Chen, J.; Hua, L.; Li, S.; Zhang, X.; Sheng, W.; Cao, S. High photocatalytic activity of hierarchical SiO₂@C-doped TiO₂ hollow spheres in UV and visible light towards degradation of RhB. *J. Hazard. Mater.* **2017**, *340*, 309–318. [[CrossRef](#)] [[PubMed](#)]
39. Liang, H.; Jia, Z.; Zhang, H.; Wang, X.; Wang, J. Photocatalysis oxidation activity regulation of Ag/TiO₂ composites evaluated by the selective oxidation of RhB. *Appl. Surf. Sci.* **2017**, *422*, 1–10. [[CrossRef](#)]
40. Munoz-Batista, M.J.; Fontelles-Carceller, O.; Ferrer, M.; Fernández-García, M.; Kubacka, A. Disinfection capability of ag/g-c₃n₄ composite photocatalysts under UV and visible light illumination. *Appl. Catal. B Environ.* **2016**, *183*, 86–95. [[CrossRef](#)]
41. Hernández, J.V.; Coste, S.; Murillo, A.G.; Romo, F.C.; Kassiba, A. Effects of metal doping (Cu, Ag, Eu) on the electronic and optical behavior of nanostructured TiO₂. *J. Alloys Compd.* **2017**, *710*, 355–363. [[CrossRef](#)]
42. Baran, E.; Yazıcı, B. Preparation and characterization of poly (3-hexylthiophene) sensitized Ag doped TiO₂ nanotubes and its carrier density under solar light illumination. *Thin Solid Films* **2017**, *627*, 82–93. [[CrossRef](#)]
43. Torres, A.; Ruales, C.; Pulgarin, C.; Aimable, A.; Bowen, P.; Sarria, V.; Kiwi, J. Innovative High Surface Area CuO Pretreated Cotton Effective in Bacterial Inactivation under Visible Light. *ACS Appl. Mater. Interfaces* **2010**, *2*, 2547–2552. [[CrossRef](#)] [[PubMed](#)]
44. Rengifo-Herrera, J.A.; Pierzchała, K.; Sienkiewicz, A.; Forro, L.; Kiwi, J.; Pulgarin, C. Abatement of organics and Escherichia coli by N, S co-doped TiO₂ under UV and visible light. Implications of the formation of singlet oxygen (1O₂) under visible light. *Appl. Catal. B Environ.* **2009**, *88*, 398–406. [[CrossRef](#)]
45. Kubacka, A.; Munoz-Batista, M.J.; Ferrer, M.; Fernández-García, M. UV and visible light optimization of anatase TiO₂, antimicrobial properties: Surface deposition of metal and oxide (Cu, Zn, Ag) species. *Appl. Catal. B Environ.* **2013**, *140–141*, 680–690. [[CrossRef](#)]
46. Liu, P.; Duan, W.; Wang, Q.; Li, X. The damage of outer membrane of Escherichia coli in the presence of TiO₂ combined with UV light. *Colloids Surf. B Biointerfaces* **2010**, *78*, 171–176. [[CrossRef](#)] [[PubMed](#)]
47. Muñoz-Batista, M.J.; Ferrer, M.; Fernández-García, M.; Kubacka, A. Abatement of organics and Escherichia coli, using CeO₂-TiO₂, composite oxides: Ultraviolet and visible light performances. *Appl. Catal. B Environ.* **2014**, *154–155*, 350–359. [[CrossRef](#)]

